ISSN: 2414-1895 DOI: 10.6919/ICJE.202605_12(5).0011

Study on the Ultimate Drop Height of Fast Reactor Fuel Assemblies

Lei Xu, Zhendong Hu*

School of Aerospace Engineering and Applied Mechanics, Tongji University, Shanghai, 200092, China

*zdhu@tongji.edu.cn

Abstract

To evaluate the drop resistance safety performance of fast reactor fuel assemblies during operation and handling, determine their safe drop height threshold, and prevent structural integrity and sealing failure caused by accidental drops, drop impact tests at various heights were conducted. By analyzing the variation laws of acceleration and strain responses with drop height, reconstructing the drop dynamic process combined with ANSYS/LS-DYNA numerical simulation, the critical drop height for collapse failure of fuel assemblies was predicted based on the super folding element theory. The results show that the peak acceleration and peak strain increase significantly with the rise of drop height. Plastic deformation occurs at the bottom of the hexagonal wrapper tube when the drop height is 1000 mm, and collapse failure takes place at the drop height of 4050 mm. Finally, the critical drop height for structural failure of fuel assemblies is determined through theoretical analysis, which provides a quantitative safety basis for their operation and layout design.

Keywords

Fast Reactor Fuel Assembly; Drop Impact Test; Numerical Simulation; Super Folding Element Theory.

1. Introduction

Global warming is affecting every region of the planet. Rising temperatures, melting glaciers, and the increasing frequency of extreme weather events are posing severe threats to human survival and development, making it urgent to address climate change. Emission reduction is the fastest and most feasible way to mitigate climate change, with the primary focus being on limiting carbon dioxide emissions-namely, reducing the use of fossil fuels such as oil, natural gas, and coal. Nuclear power offers substantial advantages in both energy output and supply stability, and is therefore one of the most promising clean energy sources capable of large-scale replacement of fossil fuels.

In China's nuclear energy development, following second- and third-generation reactor technologies, fourth-generation nuclear systems-represented by fast reactors-are expected to play a central role in the next stage of advancement. As one of the most advanced designs, sodium-cooled fast reactors have attracted extensive research worldwide, with most studies on their fuel assemblies focusing on internal flow and heat transfer phenomena. As a key component of fast reactors, fuel assemblies may experience accidental drop events during handling, transportation, or insertion and removal operations. Such incidents could lead to the release of radioactive gases from within the assembly, posing risks to both the environment and personnel safety. Therefore, the structural design of fuel assemblies must account for the potential impact of drop and collision events during refueling operations, and their effects on structural integrity. However, this aspect has been rarely addressed in

ISSN: 2414-1895 DOI: 10.6919/ICJE.202605_12(5).0011

existing studies. Investigating the mechanical response of fuel assemblies under drop impact conditions is therefore of significant importance.

Drop-impact problems of engineering products constitute an important branch of dynamics and are widely encountered across industrial sectors, including mobile phone drops, package drop tests, and the impact of liquid-storage containers, among others [1–8]. Within the nuclear engineering field, research on drop events was initially focused on the accidental dropping of spent-fuel casks and transport casks. The BAM (Federal Institute for Materials Research and Testing, Germany) [9–11] conducted drop tests on CASTOR transport casks as early as 1978. Since then, this line of research has developed rapidly, primarily relying on a combination of finite element simulations and extensive drop experiments to evaluate the safety performance of transport systems. Several experimental and numerical studies have also been carried out. In 2015, Liu [12] assessed the safety of spent-fuel storage casks under different drop scenarios. In 2021, Su et al. [13] investigated the mechanical behavior of a reactor core during free-drop events using combined drop experiments and numerical simulations. In 2023, Lan et al. [14] employed LS-DYNA to simulate the drop impact of a reactor head onto a concrete surface and analyzed the failure behavior of the concrete structure. In 2025, Peng et al. [15] proposed an equivalent drop analysis method to reduce the computational cost of simulating spent-fuel transport cask drops.

In this study, a hook-type drop testing machine is employed to conduct drop experiments on fuel assemblies at various drop heights. The strain and acceleration responses of the fuel assembly are measured under different impact conditions, and the dependence of key mechanical parameters-such as acceleration and strain-on drop height is systematically analyzed. Based on the experimental data, a numerical model of the fast reactor fuel assembly is subsequently calibrated by adjusting the damping coefficient, leading to a validated drop-impact computational model that is consistent with the experimental observations. Finally, using the theory of super-folded elements, the critical drop height at which global crushing deformation occurs is determined. These results provide a theoretical basis and quantitative support for the structural design and safety criteria of fast reactor fuel assemblies.

2. Drop Impact Experiments on Fuel Assemblies

This study focuses on the fuel assembly of the China Experimental Fast Reactor (CEFR), which consists of five main components: the handling head, a variable-thickness hexagonal duct, a thin-walled hexagonal duct, internal fuel pins, and lower end fittings. A schematic of the model is shown in Fig. 1.

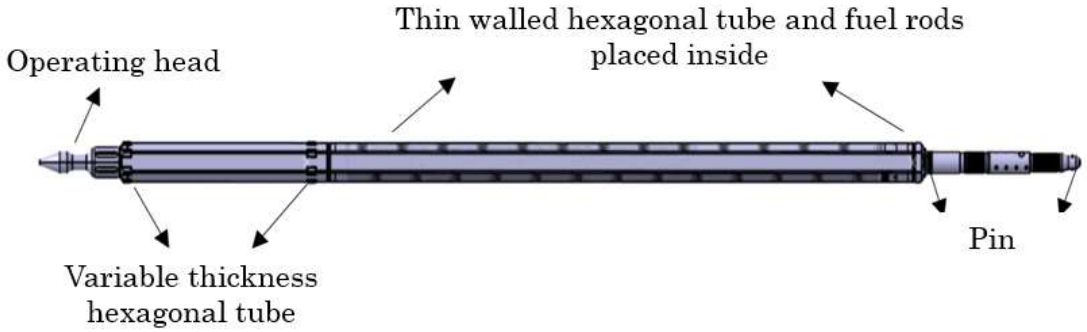

Fig. 1 Model diagram of the fuel assembly.

Strain measurement points are arranged on the central hexagonal duct at six axial cross-sections. At each cross-section, measurements are taken at three angular positions uniformly distributed at 120°. In the upper sections, three strain rosettes (orthogonal strain gauges) are installed at each level. In total, the setup includes 18 strain measurement locations and 36 strain channels. The detailed layout

ISSN: 2414-1895 DOI: 10.6919/ICJE.202605_12(5).0011

of the measurement points is shown in Fig. 2. The selected THY120-3CA strain gauges are capable of accurately capturing both plastic deformation and large-strain responses.

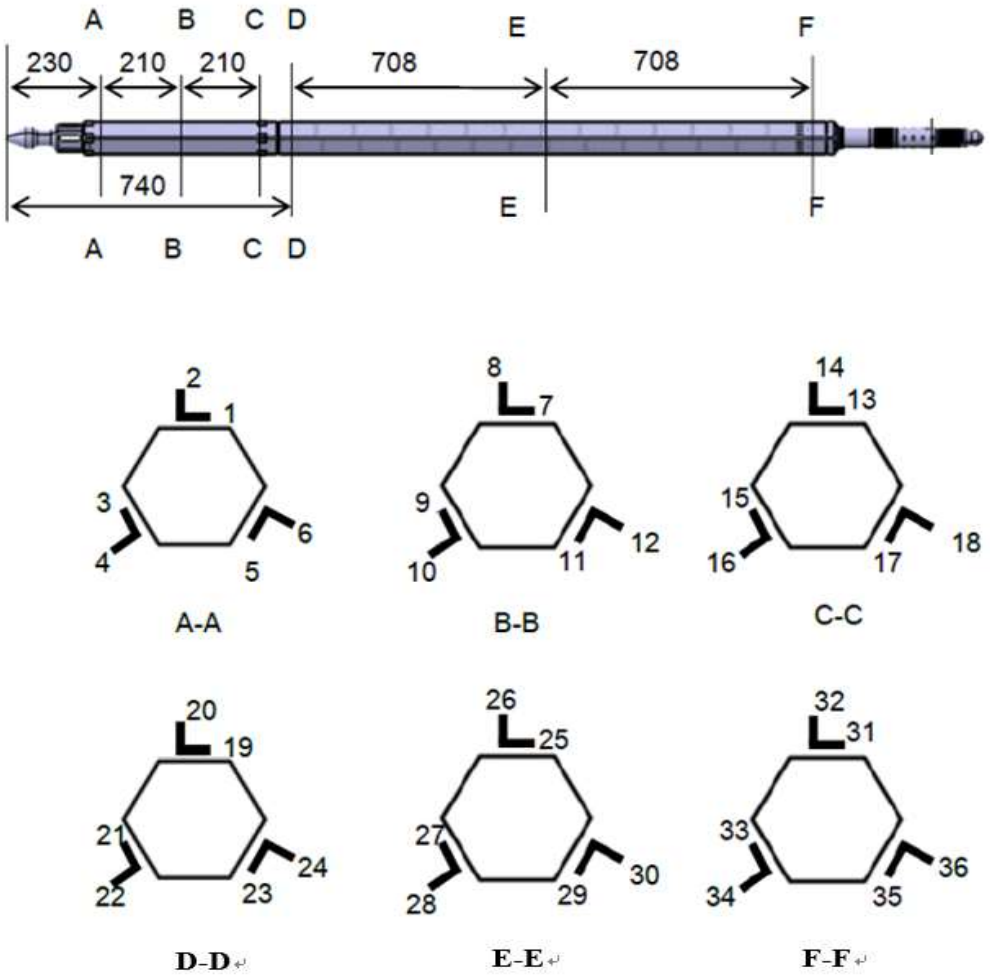

Fig. 2 Strain Gauge Placement and Numbering.

In addition to strain measurements, acceleration data were also recorded in this experiment. The acceleration response of the fuel assembly during the drop process was measured using accelerometers. Based on preliminary numerical simulations, accelerometers with a measurement range of 10,000g were selected. Two accelerometers were installed at the upper and lower edges of the hexagonal duct, respectively. The detailed sensor locations are shown in Fig. 3.

Fig. 3 Acceleration Measuring Point Layout.

ISSN: 2414-1895 DOI: 10.6919/ICJE.202605_12(5).0011

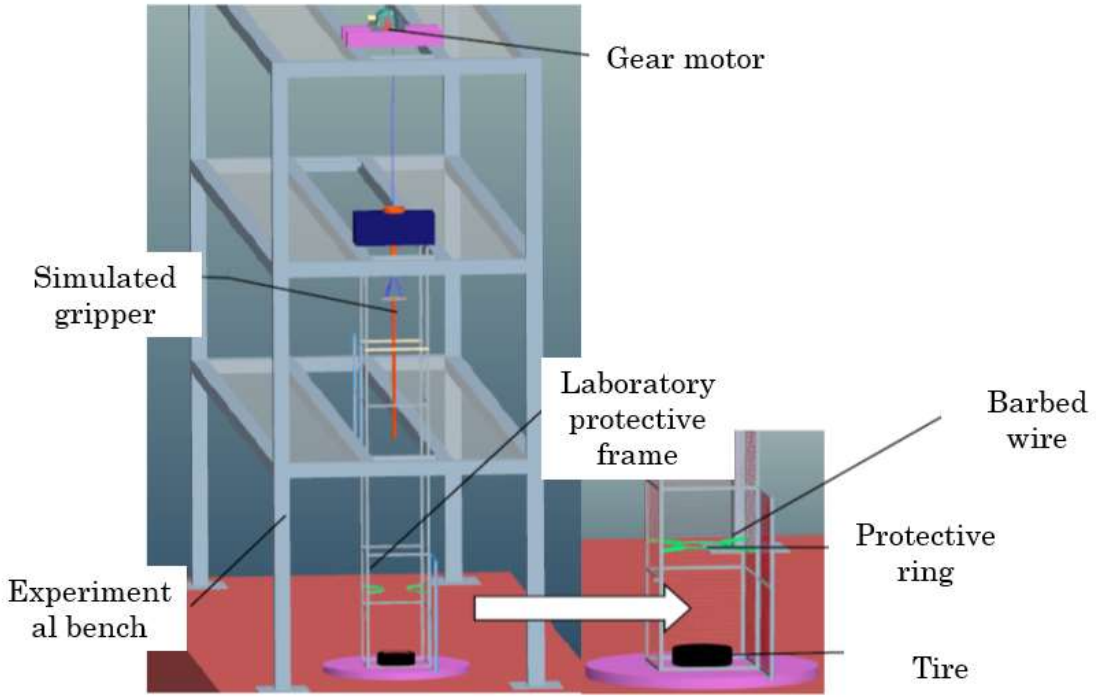

Fig. 4 Hook-type drop test machine model.

In this study, outdoor drop experiments were conducted using a hook-type drop testing machine, as schematically illustrated in Fig. 4. During the test, the fuel assembly was placed inside a protective test frame and connected at its upper end to a simulated gripping device. A geared motor was used to lift the fuel assembly to a prescribed height, ensuring a vertically aligned drop configuration. The simulated gripping mechanism was then triggered by a switch to release the assembly, allowing it to undergo free fall from rest (zero initial velocity). The assembly subsequently impacted a steel plate installed on the ground. Drop tests were performed at heights of 100 mm, 200 mm, 300 mm, 400 mm, 500 mm, 600 mm, 700 mm, 800 mm, 900 mm, and 1000 mm. During each test, both strain and acceleration data were synchronously recorded.

3. Drop Impact Simulation of Fuel Assemblies

In this study, ANSYS/LS-DYNA is employed to simulate the drop accident of the fuel assembly during handling and insertion/removal operations, in which the assembly undergoes free fall from different heights and subsequently impacts a rigid ground surface. The fuel assembly is made of a special stainless steel. During the drop impact process, large deformation and plasticity are expected, and the effect of strain rate must be considered. Therefore, a rate-dependent elasto-plastic constitutive model with kinematic hardening is adopted. This material model can incorporate isotropic hardening, kinematic hardening, or a combined isotropic–kinematic hardening formulation, and is capable of accounting for strain-rate effects as well as material failure. The main material parameters for each component are summarized in Table 1.

In the Plastic Kinematic model implemented in ANSYS/LS-DYNA, in addition to the parameters listed above, strain-rate-dependent coefficients C and P must also be defined. Based on the stress–strain curve of 1018 steel, the strain-rate parameter C is taken as 40.0 and the parameter P is set to 5.0. To ensure that the overall stiffness of the model remains unchanged and that the geometric features of key regions are preserved, several simplifications are introduced. These include removing small chamfers, surface roughness, and minor holes in the lower end fittings and handling head. In addition, the fuel pins inside the thin-walled hexagonal duct are numerous and geometrically complex. Since the present study focuses on the external cladding response under drop impact, the internal fuel elements are treated as an equivalent lumped mass. During the simulation, potential shell element

ISSN: 2414-1895 DOI: 10.6919/ICJE.202605_12(5).0011

warping must be considered. The Belytschko–Wong–Chiang shell formulation is therefore adopted, as it provides more accurate warping behavior compared with other shell formulations. For the Shell163 element, real constants are defined with a shear correction factor SHRF of 5/6, five integration points through the thickness, and a wall thickness of 0.0012 m.

Table 1. Main parameters of the material models for each component part.

Component Name	Young's Modulus (Pa)	Density(kg/m^3)	Poisson's Ratio	Yield Stress(Pa)	Tangent Modulus(Pa)
Hexagonal Duct	1.708×10^{11}	8000.0	0.260	5.756×10^{8}	4.438×10^{8}
Lower End Fitting	2.034×10^{11}	8000.0	0.256	2.304×10^{8}	6.860×10^{8}
Handling Head	2.034×10^{11}	8000.0	0.256	2.304×10^{8}	6.860×10^{8}
Fuel Pin	1.708×10^{11}	6067.1	0.260	5.756×10^{8}	4.438×10^{8}

In ANSYS/LS-DYNA dynamic analysis, the time step is automatically determined by the software and is governed by the smallest element size in the mesh. A smaller minimum element size leads to a smaller time step and significantly longer computational time. Conversely, excessively large elements may compromise solution accuracy. Therefore, the mesh is carefully optimized by balancing element size and quality. The minimum element size is increased as much as possible without affecting accuracy, in order to improve computational efficiency. Based on these considerations, a finite element model of the fast reactor fuel assembly is established. The model consists of 148,666 elements in total, including 27,504 shell elements and 121,162 solid elements. The overall finite element model is shown in Fig. 5.

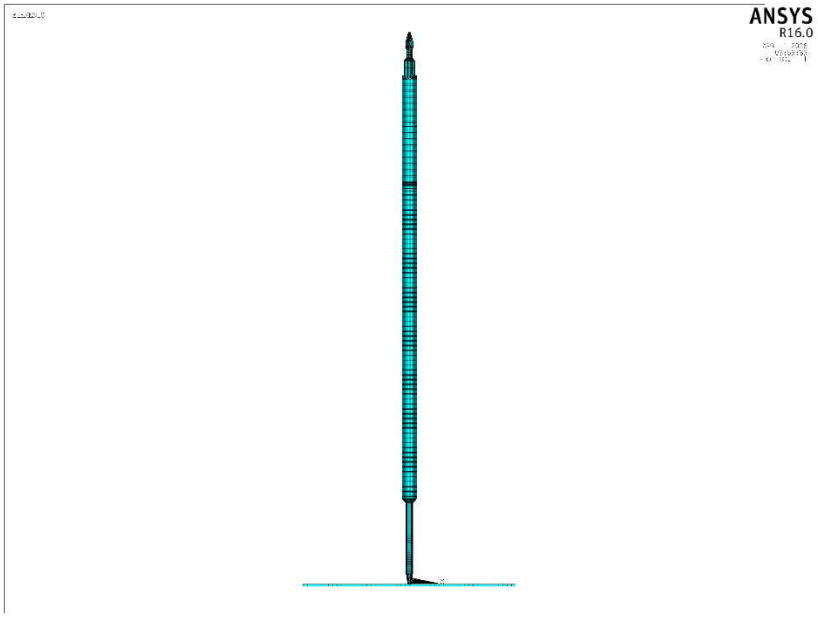

Fig. 5 Overall Finite Element Model of the Fuel Assembly.

In the contact definition, the ground is modeled as a rigid body with all degrees of freedom fully constrained (DOF = 0). The interaction between the fuel assembly and the ground is defined using automatic node-to-surface contact (ANTS). The contact between the fuel pins and the thin-walled hexagonal duct is modeled using automatic surface-to-surface contact (ASTS), with a static friction coefficient of 0.35, a dynamic friction coefficient of 0.30, and a viscous damping coefficient set to 20%. During the drop impact process, the intermediate thin-walled hexagonal duct may undergo plastic buckling and wrinkling. To account for such potentially complex and unpredictable self-

ISSN: 2414-1895 DOI: 10.6919/ICJE.202605_12(5).0011

contact behavior, automatic single-surface contact (SS) is applied to this component. To adequately capture the transient impact response while maintaining computational efficiency, the simulation time is carefully selected. Based on estimates of stress-wave propagation in the fuel assembly, the characteristic wave period is approximately 0.002 s. In addition, experimental observations indicate that the primary impact event lasts about 0.004 s. Therefore, the total simulation time is set to 0.005 s. For post-processing, both the result file (RST) and the history output file (HIS) are configured with 200 output steps to ensure sufficient temporal resolution during the solution process.

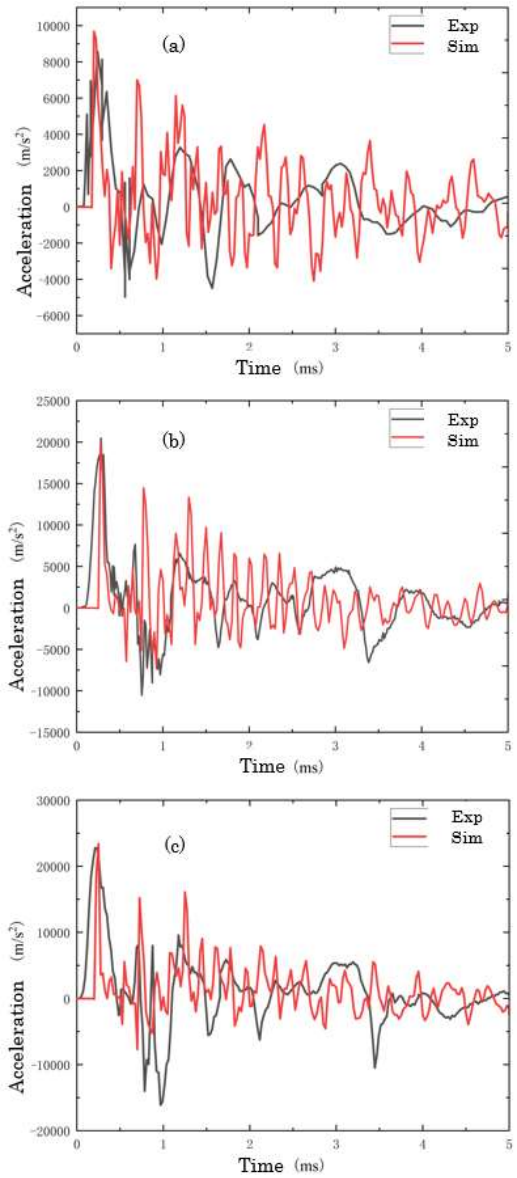

Fig. 6 Time history of acceleration response under drop impact at Measuring Point 1 (a) Acceleration at Measuring Point 1 with Drop Height 100 mm. (b) Acceleration at Measuring Point 1 with Drop Height 500 mm. (c) Acceleration at Measuring Point 1 with Drop Height 1000 mm.

4. Results

Damping represents the energy dissipation capacity of a structure or material during vibration and impact processes, in which kinetic energy is converted into thermal energy. As an intrinsic dynamic property of the structure, damping must be properly considered in both experimental interpretation and numerical simulations. In finite element dynamic analysis, the determination of damping parameters is particularly challenging. Different structures, materials, and experimental environments

ISSN: 2414-1895 DOI: 10.6919/ICJE.202605_12(5).0011

correspond to different damping characteristics. In practice, only through extensive trial calculations and comparison with experimental data can an appropriate damping representation be obtained. For the fuel assembly drop-impact problem, the collision process occurs over a very short time scale, and material damping is expected to play the dominant role. In ANSYS/LS-DYNA, damping is primarily introduced through material damping coefficients. In this study, the numerical model is calibrated by adjusting the damping coefficient. A series of parametric simulations shows that when the material damping coefficient is set to 0.2, the numerical results are in good agreement with the experimental measurements, as shown in Figs. 6–10. Overall, the simulation results are consistent with the experimental observations.

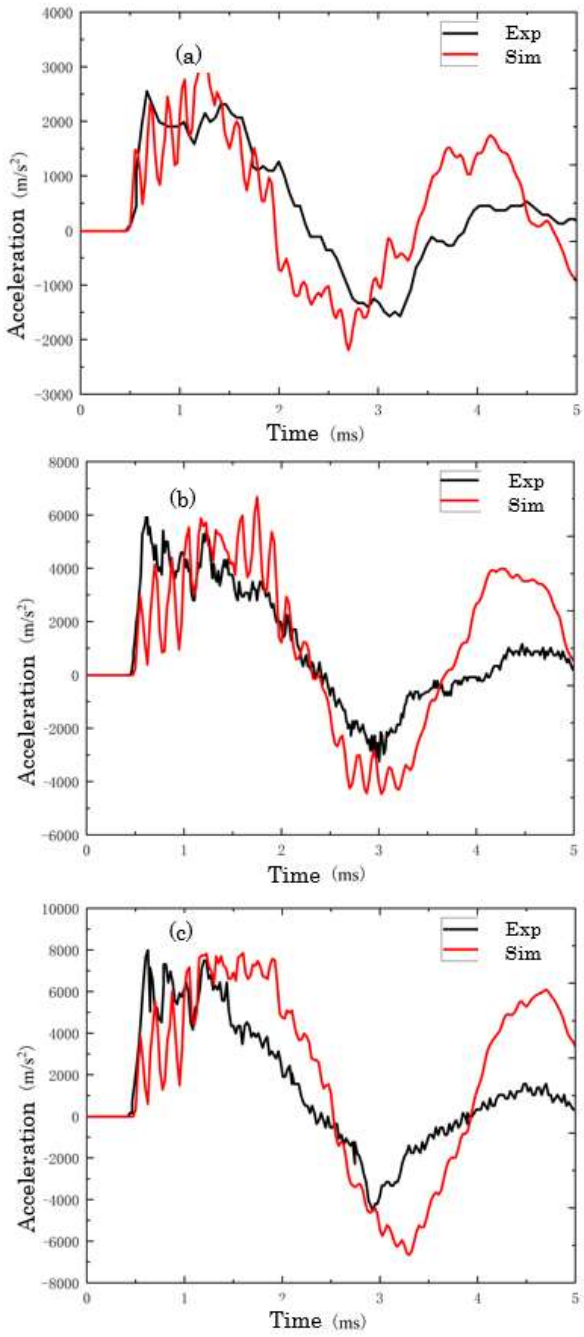

Fig. 7 Time history of acceleration response under drop impact at Measuring Point 2. (a) Acceleration at Measuring Point 2 with Drop Height 100 mm. (b) Acceleration at Measuring Point 2 with Drop Height 500 mm. (c) Acceleration at Measuring Point 2 with Drop Height 1000 mm.

ISSN: 2414-1895 DOI: 10.6919/ICJE.202605_12(5).0011

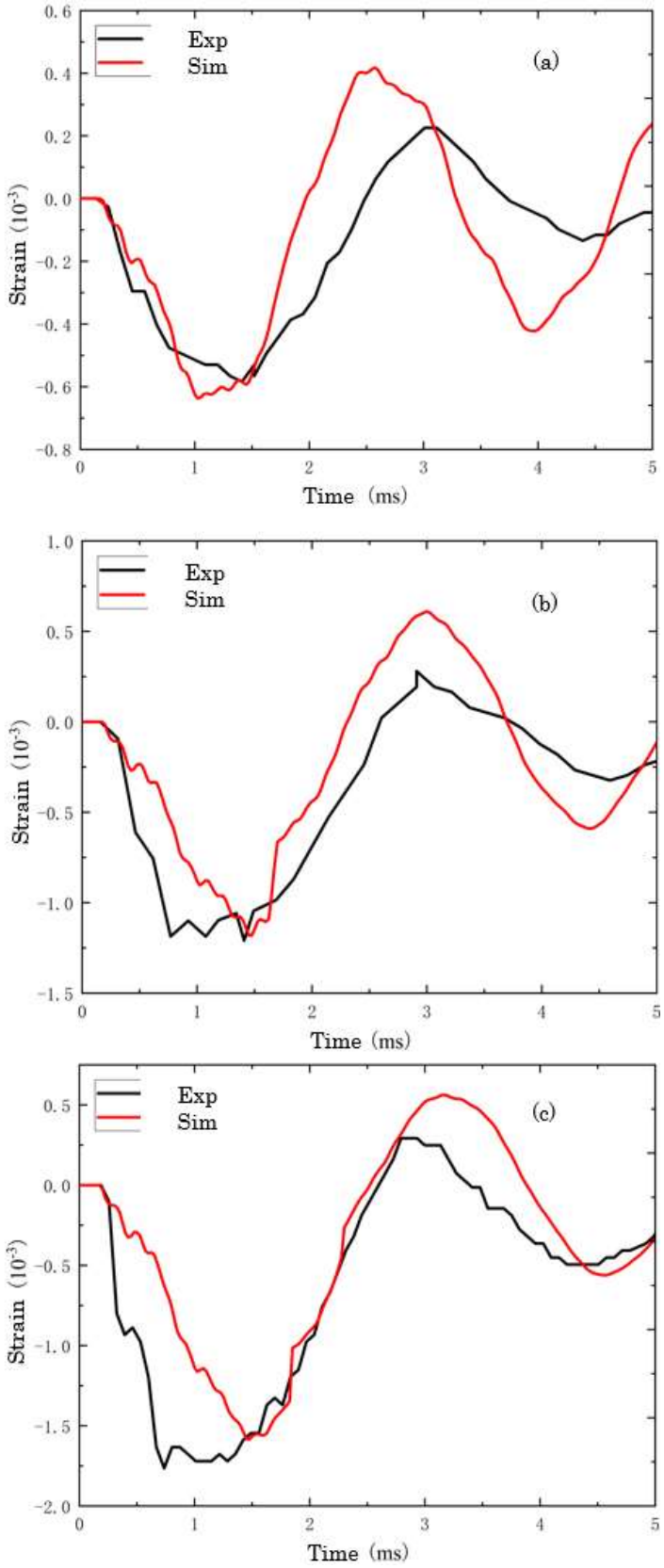

Fig. 8 Axial strain response time history of drop impact at Section E-E. (a) Axial Strain at Cross-Section E-E with Drop Height 100 mm. (b) Axial Strain at Cross-Section E-E with Drop Height 500 mm. (c) Axial Strain at Cross-Section E-E with Drop Height 1000 mm.

ISSN: 2414-1895 DOI: 10.6919/ICJE.202605_12(5).0011

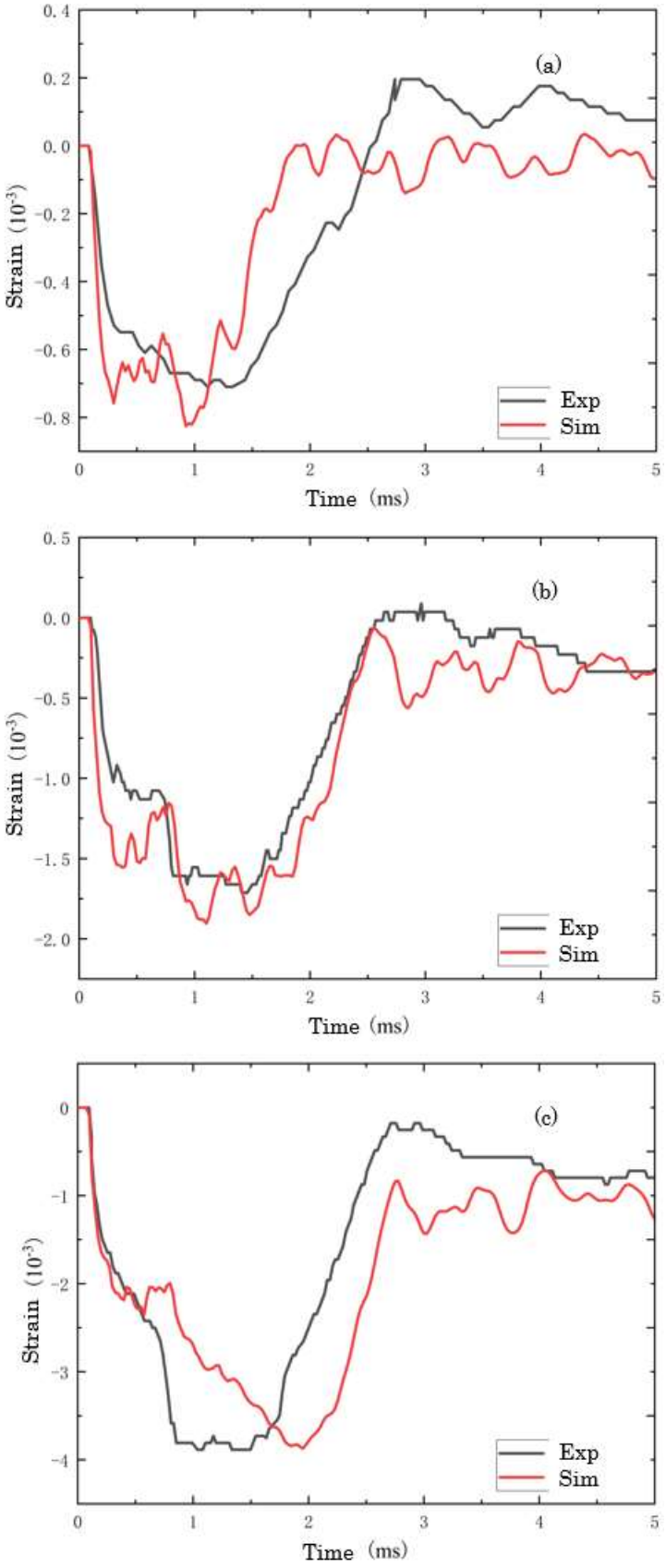

Fig. 9 Axial strain response time history of drop impact at Section F-F. (a) Axial Strain at Cross-Section F-F with Drop Height 100 mm. (b) Axial Strain at Cross-Section F-F with Drop Height 500 mm. (c) Axial Strain at Cross-Section F-F with Drop Height 1000 mm.

ISSN: 2414-1895 DOI: 10.6919/ICJE.202605_12(5).0011

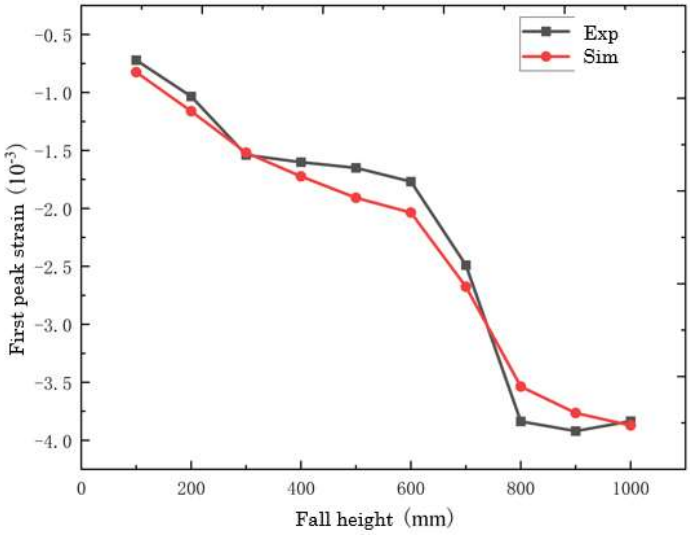

Fig. 10 Curve of first peak strain at Section F-F versus drop height.

Measurement points 1 is located above the lower end fitting, near the hexagonal duct, while measurement point 2 is positioned near the upper flange region. The first peak acceleration responses at these two locations, as a function of drop height. It can be observed that the impact acceleration of the fuel assembly increases with increasing drop height; however, the rate of increase gradually diminishes as the height continues to increase.

The first peak acceleration at measurement points 1 is significantly higher than that at measurement point 2, and the difference between the two increases with drop height. Specifically, the first peak at point 1 is approximately three times that at point 2. Moreover, the time interval between the positive and negative acceleration peaks at point 1 is noticeably shorter than that at point 2.

Since the two measurement points are located at opposite ends of the central hexagonal duct, the duct not only reduces the peak acceleration at measurement point 2, but also substantially delays the transition from the first peak acceleration to the subsequent positive peak response.

When the drop height reaches 1000 mm, the maximum axial strain at section E–E is 1800 με, corresponding to an axial stress of 307.44 MPa. At section F–F, the maximum axial strain reaches 3835 με, corresponding to an axial stress of 655.02 MPa. The maximum axial stress at section E–E is below the material yield strength, whereas the stress at section F–F exceeds the yield strength of 575.6 MPa, indicating that plastic deformation occurs at section F–F.

Metal thin-walled structures are widely used as energy-absorbing and buffering components to enhance structural safety [16–17]. In the fuel assembly, a section of thin-walled hexagonal duct is present. When the drop height is sufficiently large, this thin-walled segment may undergo progressive crushing deformation, thereby compromising the structural integrity of the fuel assembly. To ensure the safety of the assembly under drop conditions, it is necessary to determine the critical height at which crushing initiates. In this chapter, the super-folded element theory combined with the calibrated numerical model is employed to derive the critical drop height associated with crushing deformation of the fuel assembly.

In 1983, Wierzbicki and Abramowicz proposed the super-folded element theory [18–24], which provides an analytical framework for estimating the mean crushing load of metal thin-walled structures under axial compression. The central idea of the super-folded element (SFE) theory is as follows: by analyzing the crushing behavior of many thin-shell structures, the fundamental folding deformation mode is identified. The energy dissipation of a basic folding element is then evaluated based on its deformation mechanics. Subsequently, the total number of folding elements is determined according to the overall deformation mode of the structure, allowing the total energy dissipation to

ISSN: 2414-1895 DOI: 10.6919/ICJE.202605_12(5).0011

be obtained. Finally, based on the principle of energy conservation, the relationship between the incremental internal energy and the external work is used to derive the mean crushing load.

The mean crushing load is derived based on the principle of energy conservation of the system, i.e., the work done by external forces is equal to the internal energy dissipation. The work done by the crushing force is transformed into plastic deformation energy within the structure.

For an individual folding element, the energy balance equation can be expressed as follows:

$$P_m \times 2H = E_{\text{int}} \tag{1}$$

Here, 2H represents the height of the basic folding element, P_m denotes the mean crushing load, and E_{int} is the plastic deformation energy of the structure itself. During the crushing process of a basic super-folded element, the plastic deformation energy is mainly composed of three contributions: the annular surface E_1 (energy dissipation due to plastic flow region), the cylindrical surface E_2 (energy dissipation along horizontal hinge lines), and the conical surface E_3 (energy dissipation along inclined hinge lines). Therefore, Eq. (1) can be rewritten as follows:

$$P_m \times 2H = E_{\text{int}} = E_1 + E_2 + E_3 \tag{2}$$

Here, the magnitudes of E_1, E_2, and E_3 are respectively given by:

$$E_1 = M_0 \frac{16 I_1 H b}{t} \tag{3}$$

$$E_2 = \pi c M_0 \tag{4}$$

$$E_3 = 4 M_0 I_3 (\varphi_0) \frac{H^2}{b} \tag{5}$$

Here, b is the inner radius of the annular surface, t is the wall thickness of the thin-walled structure, and c is the side length of the cross-section, i.e., the length of the horizontal hinge line. $M_0 = \sigma_0 t^2/4$ denotes the fully plastic moment. For the thin-walled hexagonal duct, six folding units are formed during the crushing process. Therefore, Eq. (2) should be modified as follows:

$$P_m \times 2H = E_{\text{int}} = 6E_1 + 6E_2 + 6E_3 \tag{6}$$

Since the energy dissipation E_2 associated with the horizontal hinge lines theoretically occurs in the vicinity of these horizontal hinges, in practice plastic deformation also develops near the vertical hinge lines. Therefore, the contribution E_2 should be taken as twice the original value. Consequently, Eq. (6) becomes:

$$P_m \times 2H = E_{\text{int}} = 6E_1 + 12E_2 + 6E_3 \tag{7}$$

ISSN: 2414-1895 DOI: 10.6919/ICJE.202605_12(5).0011

By accurately evaluating the three energy components E_1, E_2, and E_3, and substituting Eqs. (3), (4), and (5) into Eq. (7), the energy balance equation can be rewritten in an alternative form as follows:

$$\frac{P_m}{M_0} = A_1 \frac{b}{t} + A_2 \frac{c}{H} + A_3 \frac{H}{b} \tag{8}$$

Here, the parameters A_1, A_2, and A_3 are functions of $\varphi, \alpha, \beta,\ and\ \gamma$, and their specific values vary depending on the case under consideration.

During the folding and crushing process, it is assumed that each folding element deforms in an idealized crushing mode, i.e., in a manner that minimizes the mean crushing load. Under this assumption, it follows that:

$$\frac{\partial P_m}{\partial H} = 0 \tag{9}$$

$$\frac{\partial P_m}{\partial b} = 0 \tag{10}$$

By solving Eqs. (9) and (10) simultaneously, one obtains:

$$H = \sqrt[3]{A_2^2 / (A_1 A_3)} \sqrt[3]{c^2 t} \tag{11}$$

$$b = \sqrt[2]{A_2 A_3 / A_1} \sqrt[3]{c t^2} \tag{12}$$

By substituting Eqs. (11) and (12) into Eq. (8), the expression for the minimum mean crushing load can be obtained as:

$$\frac{(p_m)_{\min}}{M_0} = 3 \sqrt[3]{A_1 A_2 A_3} \sqrt[3]{c/t} \tag{13}$$

=During the drop-impact process of the fuel assembly, the kinetic energy is converted into internal energy, which is dissipated as plastic deformation energy of the structure itself. By combining Eq. (1), Eq. (11), and Eq. (13), one obtains:

$$E_{\text{int}} = P_m \times 2H = 1.5 A_2 \sigma_0 c t^2 \tag{14}$$

Here, the geometric dimensions of the thin-walled hexagonal duct in the fuel assembly are given by:

$$\begin{cases} c = 0.017 \text{ m} \\ t = 0.0012 \text{ m} \\ A_2 = 6\pi \\ \sigma_0 = 5.75 \text{ MPa} \end{cases} \tag{15}$$

ISSN: 2414-1895 DOI: 10.6919/ICJE.202605_12(5).0011

By calculation, it can be obtained that:

$$E_{\text{int}} = 398.4 \text{ J} \tag{16}$$

Based on the super-folded element theory, the crushing deformation of the thin-walled hexagonal duct occurs when its strain energy reaches a critical value (E_{int}). From an energy perspective, this criterion defines the onset of structural collapse.

Table 2. Strain energy of hexagonal tubes under different drop heights.

Fall height (mm)	Hexagonal tube strain energy (J)	error
3000	174.61	56.17%
5000	602.28	51.17%
4000	384.57	3.47%
4200	424.45	6.54%
4100	404.84	1.61%
4050	395.6	0.7%

Using the calibrated computational model, the strain energy of the thin-walled hexagonal duct under different drop heights can be evaluated. The bisection method is then employed to iteratively update the drop height until convergence is achieved, yielding the minimum height at which crushing deformation occurs. The convergence criterion is defined such that the relative error between the numerically computed strain energy and the theoretical energy value is less than 1%.

The bisection method is employed to iteratively converge the solution until the strain energy of the hexagonal duct approaches the target energy ( ). The results are presented in Fig. 11 and Table 2. As shown in Table 2, when the drop height is 4050 mm, the strain energy of the hexagonal duct reaches 395.6 J, with an error of 0.7%, which satisfies the required accuracy.

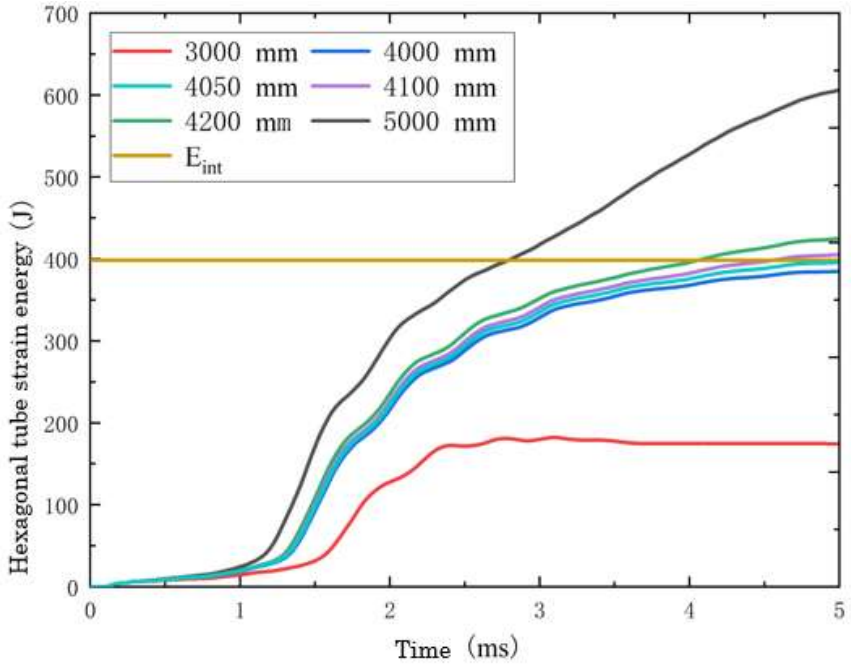

Fig. 11 Strain energy of hexagonal tubes under different drop heights.

ISSN: 2414-1895 DOI: 10.6919/ICJE.202605_12(5).0011

Fig. 12 Simulation and experimental results at a drop height of 4050 mm.

By combining the bisection method with the super-folded element theory, the critical drop height at which crushing deformation occurs in the intermediate thin-walled hexagonal duct of the fuel assembly is determined to be 4050 mm. A drop-impact experiment at this critical height was further conducted. The experimental results, together with the plastic deformation contour of the fuel assembly at a drop height of 4050 mm, are shown in Fig. 12. The experimental observations are in good agreement with the theoretical predictions. In practical applications, the maximum operational handling height of sodium-cooled fast reactor fuel assemblies is approximately 3800 mm, which is lower than the predicted critical drop height, indicating that the design satisfies safety requirements.

5. Conclusion

Drop-impact experiments were conducted on fast reactor fuel assemblies at different heights. Analysis of the results shows that both the impact acceleration and strain peaks increase with increasing drop height. In addition, the closer the measurement location is to the lower end of the structure, the larger the recorded acceleration and strain responses. When the drop height reaches 1000 mm, plastic deformation occurs at the bottom of the hexagonal duct. The numerical model is further calibrated by adjusting the material damping coefficient. It is found that when the damping coefficient is set to 0.2, the simulation results agree well with the experimental data. Based on the modified computational model and the theory of super-folded elements, the critical drop height of the fast reactor fuel assembly is predicted to be 4050 mm, which is consistent with experimental observations. Overall, the results of this study provide a theoretical basis and quantitative support for the structural design and safety criteria of fast reactor fuel assemblies.

References

[1] Mattila T T, Vajavaara L, Hokka J, et al. Evaluation of the drop response of handheld electronic products[J]. Microelectronics Reliability, 2014, 54(3): 601-609.

ISSN: 2414-1895 DOI: 10.6919/ICJE.202605_12(5).0011

[2] ZHANG Z Y, SHEN X, MO Z, et al. Numerical Simulation of Detonation Process of Solid Rocket Motor under Impact Load[J]. Journal of Projectiles, Rockets, Missiles and Guidance, 2022, 42(03): 55-60.

[3] WU J, LU F D, WANG B, et al. Dynamic Response of Fragile Components under Continuous Drop Impact Load[J]. **Journal of Vibration and Shock**, 2023, 42(20): 275-279.

[4] LIAO S J, YANG J, FANG Z, et al. Simulation and Performance Analysis of Generator Air-Drop Drop Impact under Different Buffering Methods[J]. **Packaging Engineering**, 2024, 45(19): 334-339.

[5] SHI Y S, WANG Y J. Impact Characteristic Analysis of Composite Structure Parachute-Free Air-Drop Box[J]. **Journal of Vibration and Shock**, 2024, 43(24): 323-331.

[6] WU J H, ZHANG H, XIA Z Q, et al. Drop Strength Analysis and Optimization of Air Conditioner Outdoor Unit under Cushioning Packaging Protection[J]. Journal of Appliance Science & Technology, 2025, (04): 54-58.

[7] CUI K, ZHANG X, XIA G Z, et al. Drop Simulation Analysis of Radioactive Solid Waste Product Container[J]. **Heavy Machinery**, 2025, (02): 106-112.

[8] LI P B, WEI J B, DANG L Y. Analysis of Product Response During Drop Impact of Packages Using Two Methods[J]. **Green Packaging**, 2025, (06): 15-18.

[9] Droste B, Musolff A, Müller K, et al. Drop and fire testing of spent fuel and HLW transport casks at 'BAM Test Site Technical Safety'[J]. Packaging, Transport, Storage and Security of Radioactive Material, 2011, 22(4): 200-205.

[10] Quercetti T, Müller K, Schubert S. Comparison of experimental results from drop testing of spent fuel package design using full scale prototype model and reduced scale model[J]. Packaging, Transport, Storage and Security of Radioactive Material, 2008, 19(4): 197-202.

[11] Earl E. Recent developments in the full-scale testing of spent fuel casks[J]. Nuclear Waste Technical Review Board, 2004,22(4): 137-146.

[12] LIU X. Safety Analysis and Calculation of HTR-PM Spent Fuel Storage Tank Under Drop Conditions[D]. Tsinghua University, 2015.

[13] SU X P, SONG J R, YIN T, et al. Impact Response Analysis of Free Drop Test for CFR600 Core Assembly[J]. **Structure & Environment Engineering**, 2021, 48(03): 28-35.

[14] LAN X M, JIA J Y, DAI W Y. Analysis on Structural Integrity of Nuclear Island Building under Reactor Head Drop[J]. **Chinese Journal of Nuclear Science and Engineering**, 2023, 43(06): 1400-1408.

[15] PENG X M, LAN T B, SHENG F, et al. Equivalent Drop Analysis Method and Application of Spent Fuel Transport Cask[J]. Chinese Journal of Nuclear Science and Engineering, 2025, 45(01): 170-175.

[16] WANG Y Q, LIANG Z Y, SHI W C, et al. Research on Buffering and Energy Absorption of Thin-Walled Metal Tubes under High-G Impact Environment[J]. Journal of Projectiles, Rockets, Missiles and Guidance, 2018, 38(06): 99-102+108

[17] Ning H, Chen X, Liu Z, et al. Energy absorption of thin-walled tubes with a pre-folded origami-inspired structure[J]. Advances in Mechanical Engineering, 2025, 17(3): 1-15

[18] Alexander J M. An approximate analysis of the collapse of thin cylindrical shells under axial loading[J]. The Quarterly Journal of Mechanics and Applied Mathematics, 1960, 13(1): 10-15.

[19] Wierzbicki T, Abramowicz W. On the crushing mechanics of thin-walled structures[J]. Journal of Applied Mechanics, 1983, 50: 727-734.

[20] Abramowicz W, Wierzbicki T. Axial crushing of multicorner sheet metal columns[J]. Journal of Applied Mechanics, 1989, 56(1): 113-120

[21] Abramowicz W, Jones N. Dynamic axial crushing of square tubes[J]. International Journal of Impact Engineering, 1984, 2(2): 179-208.

[22] Abramowicz W, Jones N. Dynamic axial crushing of circular tubes[J]. International Journal of 104 Impact Engineering, 1984, 2(3): 263-281

[23] Abramowicz W, Jones N. Dynamic progressive buckling of circular and square tubes[J]. International Journal of Impact Engineering, 1986, 4(4): 243-270.

[24] Wierzbicki T, Bhat S U, Abramowicz W, et al. Alexander revisited-a two folding elements model of progressive crushing of tubes[J]. International Journal of Solids and Structures, 1992, 29(24): 3269-3288.